Control of Material Damping in High-Q Membrane Microresonators

P.-L. Yu, T. P. Purdy, and C. A. Regal

Phys. Rev. Lett. **108**, 083603 — Published 23 February 2012

DOI: 10.1103/PhysRevLett.108.083603

Control of Material Damping in High-Q Membrane Microresonators

P.-L. Yu, T. P. Purdy, and C. A. Regal
JILA, University of Colorado and National Institute of Standards and Technology, and Department of Physics, University of Colorado, Boulder, Colorado 80309, USA

We study the mechanical quality factors of bilayer aluminum/silicon-nitride membranes. By coating ultrahigh-Q Si_3N_4 membranes with a more lossy metal, we can precisely measure the effect of material loss on Q's of tensioned resonator modes over a large range of frequencies. We develop a theoretical model that interprets our results and predicts the damping can be reduced significantly by patterning the metal film. Using such patterning, we fabricate Al-Si_3N_4 membranes with ultrahigh Q at room temperature. Our work elucidates the role of material loss in the Q of membrane resonators and informs the design of hybrid mechanical oscillators for optical-electrical-mechanical quantum interfaces.

PACS number(s): 03.67.-a, 42.50.-p, 85.85.+j, 46.40.Ff

Silicon nitride membranes have recently emerged as promising resonators for applications ranging from precision sensing to realization of a mesoscopic quantum harmonic oscillator [1–3]. Because of their large tensile stress, Si_3N_4 membranes can have MHz resonant frequencies with sub-Hz damping rates. The resulting room-temperature Q-frequency products of above 10^{13} Hz approach the performance of quartz oscillators [4]. This ultrahigh Q combined with a two-dimensional geometry is an ideal platform for control and detection of motion in a high-finesse Fabry-Pérot cavity, and cooling Si_3N_4 membranes in such cavities to their quantum-mechanical ground state is a near-term prospect. However, the mechanisms that limit the realized Q-factors of these tensioned resonators are just beginning to be explored [5–8].

To date, studies have focused on pure dielectric Si_3N_4 membranes, but a variety of proposed cavity mechanics experiments would be enabled by the addition of a metallic layer to Si_3N_4 while maintaining high Q [9–12]. Foremost, a metallic membrane section could form a capacitor plate that couples to a microwave LC resonator; in fact, pure metallic drums have recently been ground-state cooled using a combination of cryogenic and microwave cavity cooling [9]. With a hybrid dielectric/metallic membrane, one could couple mechanical motion simultaneously to optical light and a microwave electrical circuit in the quantum regime [10]. Such a device could solve the difficult, yet crucial, problem of transferring quantum states between microwave and optical photons. It could also enable enhanced detection of excitations in a room-temperature electrical circuit via photodetection [11]. Further, a magnetic metallic film could be used for magnetic coupling of spins to membrane motion [12]. However, the success of these applications will hinge on creating hybrid membranes with a sufficiently high quality factor at relevant temperatures.

In our work, we add metallic thin films to Si_3N_4 membranes and explore the quality factor of many spatial modes of the membranes (Fig. 1). First, we identify two distinct loss mechanisms in our experiments: (1) loss of energy from the mechanical mode into the substrate, i.e. radiation loss, and (2) material damping due to the lossy metallic film. Then, we isolate the material loss-limited Q and develop an anelastic theory that explains the observed dependence of Q on frequency

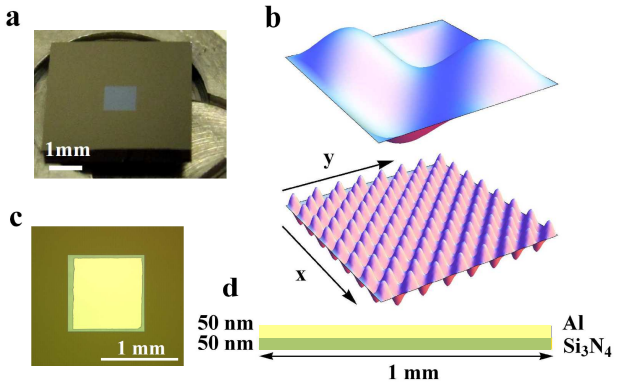

FIG. 1: (color online). Geometry of membrane modes. (a) Image of a 1 mm membrane in its silicon frame. (b) Illustrations of the $(m, n) = (2, 2)$ and $(15, 15)$ modes. (c) Image of a patterned Al film on top of Si_3N_4. The central square is Al and the rim is Si_3N_4 suspended on a Si frame. (d) Schematic diagram of the Al/Si_3N_4 bilayer membrane (50 nm Al and 50 nm Si_3N_4).

for a general clamped, lossy membrane. Our work clarifies the role of material loss in highly-stressed two-dimensional resonators, and has significant predictive power. Finally, we calculate and demonstrate that by removing the metal in a very small region near the clamp, we can create metallic Si_3N_4 membranes with impressive quality factors of over 5×10^6 at 1 MHz at room temperature.

We use 50 nm-thick stoichiometric LPCVD nitride membranes that are supported by a 200 μm-thick silicon frame (from Norcada Inc.). The membranes are in a square geometry of side length $l = 0.5$ mm or 1 mm with tensile stress $\sigma \sim 0.9$ GPa and mass density $\rho \sim 2.7$ g/cm^3. The membrane mode shapes are given by approximately sinusoidal functions like those shown in Fig. 1(b) with resonant frequencies $f_{mn} \sim \sqrt{\sigma(m^2 + n^2)/4\rho l^2}$, where m, n are the integer mode indices representing the number of antinodes. The silicon frame is glued at three corners to a metal form on a piezoelectric actuator. To probe the mechanical displacement, we position the membrane at the end of one arm of a Michelson interferometer. We characterize the mechanical quality factor

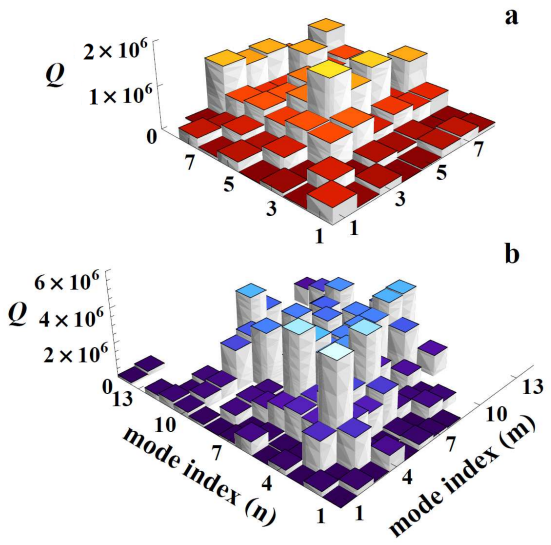

FIG. 2: Radiation loss for a square membrane. Measurements of quality factors for many different modes of an (a) 0.5×0.5 mm and (b) 1×1 mm Si_3N_4 membrane. The symmetric modes generally have higher Q than asymmetric modes, as predicted by a radiation loss model [5].

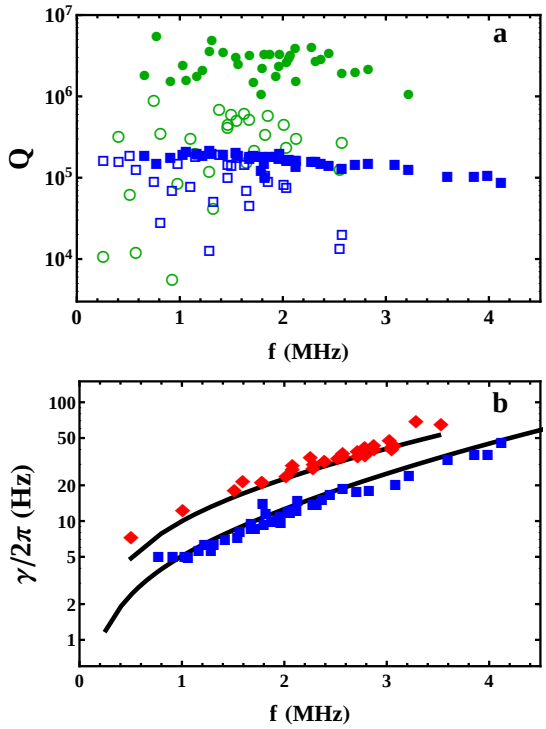

FIG. 3: Extracting the material loss-limited Q. (a) Measured quality factors of a square Si_3N_4 membrane before (green circles) and after (blue squares) adding a 50 nm film of Al. The modes limited (not limited) by radiation loss are marked by open (closed) circles. The data are plotted as a function of frequency measured after adding the Al. (b) Mechanical linewidth of the modes limited by the material loss of Al for 0.5×0.5 mm (red diamonds) and 1×1 mm (blue squares) membranes. To compare to theory, we calculate the damping rate $\gamma_{mn}/2\pi$ for each mode, and the points are connected with the displayed lines.

by monitoring the ringdown of the mechanical excitation as a function of time in vacuum of less than 10^{-6} torr.

In a first experiment, we measured the Q's of pure Si_3N_4 membranes. As shown in Fig. 2, we have the ability to measure the quality factors of many modes (up to 150) with different symmetries and to confidently assign a mode (m, n) to all measured points. When the data are plotted versus resonant frequency (green circles in Fig. 3), the Q is non-monotonic. However, when the data are plotted as a function of mode index in each dimension (Fig. 2), we see that the asymmetric modes (indices n and m dissimilar) have strikingly smaller quality factors than do the more symmetric modes (n and m nearly equal). This observation is consistent with expected trends for radiation loss of elastic waves through the membrane clamp. As recently calculated and measured in Ref. [5], the degree of destructive interference of elastic waves in the substrate is responsible for the symmetry dependence. While we see consistently low Q's with highly asymmetric modes, we see some variability due to the membrane mounting structure especially among the lowest order modes [6], as expected for a radiation loss mechanism [8]. However, for the high-order symmetric modes that asymptote to Q's over a million, it becomes unclear whether radiation or material loss is the dominant effect.

In our next experiments, we deposit 50 nm of Al using e-beam evaporation on top of the pure Si_3N_4 membrane measured in Fig. 2(b). The membrane remains under large tensile stress, but adding the additional film does decrease the effective stress to $\sigma_{\rm eff} = 0.35$ GPa. With the addition of the metal, we see a drop in Q to a maximum of $\sim 2 \times 10^5$ as shown in Fig. 3(a). Again, as a function of frequency, the Q's are non-monotonic, but by drawing on our knowledge of the Q's of the pure Si_3N_4 membrane [Fig. 2(b)], we can clearly distinguish radiation loss and material loss. The open squares in Fig. 3(a) represent the asymmetric modes found to be radiation-loss limited for the pure Si_3N_4 membrane. If we remove these points from the Al-Si_3N_4 membrane measurements, we arrive at a clean set of points (closed squares) representing the material loss-limited Q as a function of frequency. Damping rates $\gamma = 2\pi f/Q$ for two datasets obtained using this method are shown in Fig. 3(b).

We have developed a theoretical framework to describe the frequency dependence of the material loss-limited quality factors of our two-dimensional structures. We model the membrane as an anelastic plate that dissipates mechanical energy under cyclic loading [13]. Under oscillation, the material's strains and stresses are not in phase, and the energy supplied by the out-of-phase stresses is converted irreversibly to heat. This picture has been successfully developed to understand damping in one dimensional Si_3N_4 strings [14, 15].

In our case, we start by applying standard plate theory with an in-plane force [16], i.e., under tensile stress, to determine the normal modes. The modes must satisfy the boundary conditions of the clamped plate $W=(\partial/\partial x)W=0$ or $W=(\partial/\partial y)W=0$ for all four edges. We express the 2D mode function $W_{mn}(x,y)$ as a product of stressed-beam functions $u_m(x)u_n(y)$. We have verified the accuracy of this description via perturbation theory [17]. We use a closed-form expression for the function $u_n(x)$ that is a sinusoid with an exponential correction near the edge for the clamped boundary condition.

For each mode, we can calculate the loss due to anelasticity. The oscillation of the plate induces oscillating strains $\varepsilon_{xx}e^{i\omega t}$, $\varepsilon_{yy}e^{i\omega t}$, and $\varepsilon_{xy}e^{i\omega t}$, and the accompanying stresses are given by the usual constitutive equation of classical plate [18] with the complex Young's modulus $\tilde{E}=E_1+iE_2$, where E_2 is called the loss modulus. During one cycle, the full expression for the energy lost is

$$\Delta U=\int \frac{2\pi E_2(x,y)}{1+\nu}\left\{\frac{(\varepsilon_{xx}+\varepsilon_{yy})^2}{2(1-\nu)}+\frac{\varepsilon_{xy}^2}{4}-\varepsilon_{xx}\varepsilon_{yy}\right\}dV \quad (1)$$

where ν is the Poisson's ratio [17]. Note, the strain term $\varepsilon_{xx}=-z(\partial^2 W/\partial x^2)$ is proportional to the curvature of the mode function. To calculate the quality factor, we also need an expression for the total stored energy. It can be obtained from the maximum kinetic energy $U=2\rho\pi^2 f^2\int W(x,y)^2 dV$. The quality factor for a particular mode W_{mn} is then given by $Q_{mn}=2\pi U_{mn}/\Delta U_{mn}$.

We start by using our theory to calculate the damping of fully-metallized membranes. We apply a least-squares fit to the two datasets (two different-sized membranes) in Fig. 3(b) assuming a single frequency-independent loss modulus. This reveals an effective bilayer $E_2=0.55$ GPa. The corresponding Al loss modulus is consistent with typical values for thin-film polycrystalline Al at room temperature, as measured, for example, via depositing Al on a low-loss Si cantilever [19]. The presumed microscopic origin of the loss is related to crystallographic defects such as grain boundary sliding [20, 21] or kinks on dislocations [22]. Despite this underlying complexity, our model assumes very little about the microscopic origin of the loss. Namely, we assume that the defects are uniformly distributed within the deposited metal in the x and y directions. We also assume the temperature stays sufficiently constant in our measurements so as not to affect the loss modulus. We have verified that the heating due to our measurement laser of power 150 μW is not a significant effect by measuring constant quality factors as the power is varied from 10 to 900 μW.

With continued analysis of the theory we can not only model, but understand the Q dependencies seen in Fig. 3, and put our observations in the context of other studies in 1D and 2D [5, 8, 14, 15]. We would like to understand: (1) The frequency dependencies, i.e., why an extremely corrugated mode has only a slightly lower Q than the fundamental mode in our measurements (2) The geometry dependence, i.e., how damping should scale with resonator size. First, we address the frequency dependence. As noted above in the discussion of Eq. (1), the loss is given by an integral of terms proportional to the mode curvatures. We identify two contributions to the curvature, namely that induced at the clamped edge and that near the antinodes in the interior of the membrane. If the curvature at the edge dominates we expect a flat Q as a function of frequency, or if the antinode contribution dominates we expect a decreasing Q as the frequency (and correspondingly the number of antinodes) increases. We quantify these statements by deriving a simplified expression for Q as a function of mode indices m and n for the limit of (1) an isotropic membrane, i.e. constant E_2 in x and y and (2) high-stress quantified by small λm and λn where $\lambda=\sqrt{E'h^2/3\sigma l^2}$ is a dimensionless stress parameter. Here $E'=E_1/(1-\nu^2)$ and h, l, and σ are the height, length, and stress of the membrane respectively. In these limits, Eq. (1) becomes an integral over squared sinusoidal terms (antinode contribution) and an exponential term (edge contribution) to give a total Q of [17]

$$Q_{mn}\sim\frac{1}{\lambda}\frac{E_1}{E_2}\left(\underbrace{1}_{\text{edge}}+\underbrace{\lambda\frac{(m^2+n^2)\pi^2}{4}}_{\text{antinode}}\right)^{-1} \quad (2)$$

The term $\lambda(m^2+n^2)\pi^2/4$ determines whether there will be a frequency-dependent Q. For our experiments, and similar experiments with large membranes [5, 8], $\lambda\sim 10^{-4}$–10^{-3}, and hence we expect a relatively flat Q. However, if the edge length is decreased, λ increases and the antinode contribution can become large. Hence, a frequency dependence appears for experiments such as those in Ref. [14] where shorter strings (<35 μm) are used.

Further, the prefactor $1/\lambda$ in Eq. (2) determines the geometry and stress dependence for the Q of the fundamental mode. Physically, λ can be written as the ratio of bending energy to elongation energy [17], and as discussed in Ref. [14], exciting energy in the form of elongation energy rather than bending energy leads to higher Q. More concretely, based upon Eq. (2), we predict that if the membrane side length l is doubled, Q of the fundamental mode will double for the same loss modulus, and this is exactly what is observed in Fig. 3(b); the analogous effect in 1D was observed in Ref. [14]. We also see that as the stress is varied, Q scales with $\sqrt{\sigma}$, and hence the linewidth $\gamma=2\pi f/Q$ remains constant. While Eq. (2) only holds in the stressed limit, a calculation in the zero stress (flexural) limit reveals the linewidth increases by a only a few factors from the highly-stressed case.

Our analysis above indicates that by making the loss modulus near the membrane edge small, we can reduce the loss significantly. Using our ability to control the addition of material loss with the Al film, we can directly test this prediction. The inset to Fig. 1(c) shows a 1×1 mm membrane where we deposited Al nearly everywhere except in a small $\sim$50 μm region near the edge. The quality factors of this membrane were measured to be dramatically higher (blue circles) than a control experiment (red squares) in which an identical layer of Al was deposited everywhere on a separate membrane (Fig. 4).

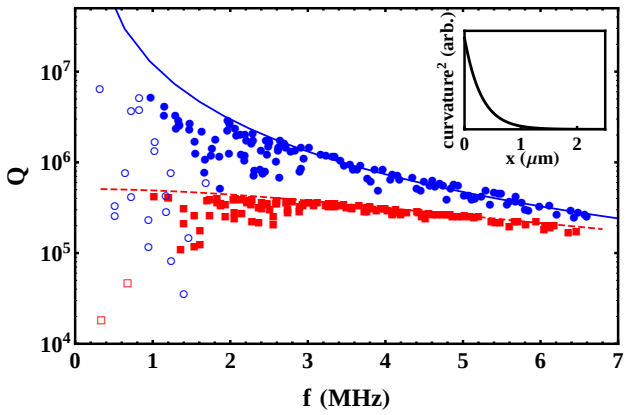

FIG. 4: (color online). Ultrahigh-Q metal-covered membranes. Measured quality factors of two Si_3N_4 membranes with Al everywhere but near the edge of the membrane (blue circles) [see Fig. 1(c)] and a full film of Al as a control experiment (red squares). Asymmetric modes (with one mode index less than or equal to two) are marked by open circles or open squares. Calculated quality factors for each geometry are shown by the two lines; a single loss modulus is used for both. (Inset) The square of the curvature of a stressed mode as a function of distance along one coordinate of the membrane. This function decays exponentially near the membrane edge.

For these data we show the Q's measured for all modes, but identify the lower-Q asymmetric modes by open circles or squares. For both datasets in Fig. 4 we anneal the membranes at 340°C after depositing the Al film resulting in an effective stress of $\sigma_{\rm eff} = 0.6$ GPa. While annealing was not necessary for studying the fully-metallized membranes of Fig. 3, the unequal stress of the Al film in the partially-metallized membrane makes the higher-order modes difficult to identify. The annealing mitigates this problem, but we still cannot identify modes past 3 MHz. Hence past this point we analyze the Q envelope by measuring the highest Q mode in every 50 kHz window.

We can again apply our theory to quantitatively predict the Q for this new geometry. Since E_2 now becomes a function of position on the membrane, we return to using the full expression of Eq. (1). We assign a finite loss modulus for the Al region and zero loss for the Si_3N_4 rim. We approximate the mode functions as those expected for a uniformly stressed membrane. This reveals the solid line in Fig. 4, which we find scales as $1/n^2$ for diagonal modes, as expected from antinode contributions. The dashed line shows the corresponding result for the fully metallized membrane using the same loss modulus. (The loss modulus found here is $E_2 = 0.3$ GPa, which is a smaller value than for Fig. 3 due to the annealing.) We find the theory successfully traces out the envelope of the measured Q's. The lowest order modes of the partially-metallized membrane reach as high as $Q = 6.5 \times 10^6$; this falls short of the predicted Q just from Al material loss (blue line) likely because these modes are now again limited by radiation loss. In comparison, recent measurements of metal microstrings at room temperature revealed Q's of 10^3–10^5 [23, 24], and even at cryogenic temperatures, where the metal's material loss is significantly reduced, observed Q values for tensioned microresonators are typically $10^5 - 10^6$ [25–27].

It is elucidating to understand what would happen to the Q trends we observe for the partially-metallized membrane upon varying the membrane stress. This requires analysis of the spatial dependence of the curvature in the membrane plane. In the inset to Fig. 4 we see the high-curvature area only occupies a very small ~ 1 μm region near the edge of a high-tension membrane (here we use our lowest $\sigma_{\rm eff} = 0.35$ GPa); specifically, the decay length is $\lambda l/4$ [17]. As the stress is reduced (and hence λ is larger), the curvature becomes more uniformly distributed over the membrane plane. Hence we would not expect a dramatic difference in Q for a purely flexural mode when avoiding lossy material only at the edge.

The localized curvature of the tensioned membrane that we observe provides insight into a variety of membrane applications. Note for higher-order two-dimensional modes the curvature varies along the edge of the membrane, i.e. there are low-curvature regions near the nodes at the membrane edge [17]. Thus, to create an electrical link between a central metallized patch and external circuits, and maintain high-Q performance, one could tailor metal connections to match up with the low-curvature regions near nodes at the membrane edge [17]. Further, membrane patterning via holes is a promising technique to increase reflectivity of membranes for optomechanics experiments, but like metal deposition, also has potential to introduce defects. A full understanding of the curvature of the two-dimensional membrane is important for understanding the change in Q, or a lack of a decrease in Q, in recent patterning experiments [28, 29].

We thank I. Wilson-Rae, K. W. Lehnert, and R. W. Simmonds for valuable discussions and A. M. Kaufman for assistance. This work was supported by the DARPA QuASAR program, ONR YIP, and JILA NSF-PFC. CR thanks the Clare Boothe Luce Foundation for support. TP thanks the NRC for support.

[1] I. Wilson-Rae, N. Nooshi, W. Zwerger, and T. J. Kippenberg, Phys. Rev. Lett. **99**, 093901 (2007).
[2] F. Marquardt, J. P. Chen, A. A. Clerk, and S. M. Girvin, Phys. Rev. Lett. **99**, 093902 (2007).
[3] J. D. Thompson *et al.*, Nature **452**, 72 (2008).
[4] M. A. Lombardi, in *Mechatronic Systems, Sensors, and Actuators*, edited by R. H. Bishop (CRC Press, Boca Raton, 2007).
[5] I. Wilson-Rae *et al.*, Phys. Rev. Lett. **106**, 047205 (2011).
[6] D. J. Wilson, C. A. Regal, S. B. Papp, and H. J. Kimble, Phys. Rev. Lett. **103**, 207204 (2009).
[7] B. M. Zwickl *et al.*, Appl. Phys. Lett. **92**, 103125 (2007).
[8] A. Jöckel *et al.*, Appl. Phys. Lett. **99**, 143109 (2011).
[9] J. D. Teufel *et al.*, Nature **475**, 359 (2011).
[10] C. A. Regal and K. W. Lehnert, J. Phys.: Conf. Ser. **264**, 012025 (2011).
[11] J. M. Taylor, A. S. Sorensen, C. M. Marcus, and E. S. Polzik,

arXiv:1108.2035v1 (2011).
[12] P. Rabl *et al.*, Phys. Rev. B **79**, 041302 (2009).
[13] C. Zener, Phys. Rev. **53**, 90 (1938).
[14] Q. P. Unterreithmeier, T. Faust, and J. P. Kotthaus, Phys. Rev. Lett. **105**, 027205 (2010).
[15] S. Schmid, K. D. Jensen, K. H. Nielsen, and A. Boisen, Phys. Rev. B **84**, 165307 (2011).
[16] A. W. Leissa, *Vibration of Plates* (NASA, Washington, D.C., 1969).
[17] See supplementary material.
[18] S. Timoshenko, *Vibration Problems in Engineering* (D. Van Nostrand Company, Inc., New York, 1937).
[19] G. Sosale, S. Prabhakar, L. Frechette, and S. Vengallatore, J. Microelectromech. Syst. **20**, 764 (2011).
[20] B. Berry and W. Pritchet, Journal de Physique **42**, C5 (1981).
[21] M. Prieler, H. Bohn, W. Schilling, and H. Trinkaus, J. Alloys Compd. **211/212**, 424 (1994).
[22] F. Hoehne *et al.*, Phys. Rev. B **81**, 184112 (2010).
[23] A. K. Pandey, O. Gottlieb, O. Shtempluck, and E. Buks, Appl. Phys. Lett. **96**, 203105 (2011).
[24] T. Larsen *et al.*, Appl. Phys. Lett. **98**, 121901 (2011).
[25] M. D. LeHaye, O. Buu, B. Camarota, and K. C. Schwab, Science **304**, 74 (2004).
[26] C. A. Regal, J. D. Teufel, and K. W. Lehnert, Nature Phys. **4**, 555 (2008).
[27] J. D. Teufel *et al.*, Nature **475**, 359 (2011).
[28] U. Kemiktarak, M. Metcalfe, M. Durand, and J. Lawall, arXiv:1107.3170v1 (2011).
[29] C. H. Bui *et al.*, arXiv:1110.3625v1 (2011).